# Passive Fluidic Control of Flow around Circular Cylinder

James Ramsay*, Mathieu Sellier* and Wei Hua Ho†
*Department of Mechanical Engineering, University of Canterbury, Christchurch, New Zealand
† School of Mechanical, Industrial & Aeronautical Engineering, University of Witwatersrand, Johannesburg, South Africa

*Summary*. Suction of the boundary layer is an effective means of delaying separation and reducing drag on external flows. However, if a pumping system is required to generate the suction, the weight and power consumption of the system can undo that benefit. 'Autogenous' (self-generating) suction control is a type of flow control that utilises the energy already within a flow (notably the pressure gradients) to drive the suction, thereby requiring no further energy to the system. This paper describes numerical studies that were performed on the flow around the circular cylinder in the 2D laminar range: $Re = 40$ (steady) and $Re = 120$ (unsteady). Suction and blowing control were implemented by imposed velocity boundary conditions. These controls were then modified using optimisation methods to generate arrangements of suction and blowing that can be passively generated by their pressure differential (i.e. $P_s \geq P_b$). Steady and unsteady simulations were performed. It was found that at both $Re = 40$ and $Re = 120$ drag-reducing arrangements could be produced. At $Re = 120$ a reduction in drag of 4.3% was found while maintaining a positive pressure differential from the suction to blowing loci. This approach for developing passive suction control can be applied to other bluff body flows and higher Reynolds numbers to design efficient optimised flow control.

## Introduction

Boundary layer suction has a long history as an effective means of flow control. The first recorded use of suction to control a fluid flow was by Ludwig Prandtl to test his boundary layer theory (1). It has been shown by many experimental (2; 3; 4) and numerical (5; 6; 7; 8) studies that suction control is extremely effective at reducing drag, subduing vortex shedding, or improving lift in external flows. Additionally, optimised non-uniform suction can be much more efficient and effective than uniform suction or slot suction (9). In some applications, suction control is effective not by its influence on the boundary layer, but by its body force imposed on the flow, for example when suction is applied on the already separated wake behind an object (10).

On the other hand, to generate the suction flow, an appropriate pressure gradient is required. This pressure gradient must be sufficient to overcome porous and viscous losses through any suction ducting, and depending on the strength of suction desired, must also overpower the momentum of fluid outside the boundary layer. This is the case whether the suction is applied through slots or with a porous surface. In practice, this is typically achieved using a pump or compressor (11; 3). The energy required to power this pump may exceed the savings in energy from drag reduction. Additionally, the weight of the pump and suction system will increase the mass needed to accelerate for transportation applications. Due to this and other considerations, while suction control may be extremely effective, it may be inefficient (12).

One alternative to a pump system is to use the pressure gradients already within a flow to drive a suction/blowing through the bounding surface. This was coined 'autogenous suction control' by Atik and van Dommelen, meaning 'self-generating' (13). By connecting a region of high pressure to a region of low pressure, a secondary flow can naturally develop. Autogenous suction was first explored behind shocks (14; 15; 16), but Atik and van Dommelen were the first to explore its potential in subsonic and laminar flows.

In their numerical study, it was shown that autogenous suction control was possible for a thin airfoil and could delay separation over a range of angles of attack (13)). The autogenous suction control was achieved by applying suction over a distributed area downstream of the location of minimum pressure (and separation point) while exhausting the fluid removed by suction upstream. The numerical approach by Atik and van Dommelen was limited in that it solved the boundary layer equations rather than the full Navier-Stokes equations, which was appropriate for their idealised airfoil but is unlikely to be so for other flow cases. Additionally, their study was intentionally idealised, and many considerations of a physical implementation were ignored or set to arbitrary values (e.g. viscous and porous losses, the effect of tangential pressure gradients). However, a type of autogenous suction control device was patented by inventor Pradip Parikh and assigned to Boeing, to delay separation over an aircraft wing (17).

The paper by Atik and van Dommelen demonstrated the potential for autogenous suction to beneficially control the flow around an aerodynamic shape (delayed separation), while the patent held by Boeing demonstrates how it might be used for a real-world application (13; 17). However, it has not been shown whether autogenous suction control can reduce drag on a body, and whether other arrangements – such as suction upstream of the minimum pressure location – would be beneficial. Therefore, in this study, autogenous suction control was developed on a canonical flow with the objective to minimise drag and develop a methodology for designing autogenous suction control using the Navier-Stokes equations. A bluff body was chosen as the geometry in order to supplement the work of Atik and van Dommelen on a streamlined shape, hence, the flow around the circular cylinder in the 2D laminar range ($Re \leq 188.5$) was modelled numerically. Parameterised boundary conditions were used to impose the suction and blowing flows, which were then optimised with constraints so as to be autogenous.

## Methodology

### Computational Domain & Governing Equations

The flow around the circular cylinder was modelled numerically for $Re = 40$ and $Re = 120$ using COMSOL Multiphysics, a commercial Finite Element software package. The governing equations are the incompressible isothermal Navier-Stokes equations:

$$\frac{\partial \mathbf{u}}{\partial t} + (\mathbf{u}\cdot\nabla)\,\mathbf{u} - \nu\nabla^2\mathbf{u} + \frac{1}{\rho}\nabla p = \mathbf{f}, \tag{1}$$

$$\nabla\cdot\mathbf{u} = 0, \tag{2}$$

where **u** and $p$ are the velocity vector and scalar pressure fields respectively (the dependent variables), $\nu = \mu/\rho$ is the kinematic viscosity, $\rho$ is the fluid density, and **f** is the vector for all external forcing terms (in this case, zero). Both steady-state and unsteady simulations were employed in this study, and in the former case the time-derivatives vanish (first term of Equation (1)).

The computational domain is shown in Figure 1. This is the same as in (9), where the model was extensively validated against experimental data for drag and separation angle from the literature (18; 19; 20; 21). The flow around the circular cylinder is commonly studied, and its characteristics are well known (22). The flow is characterised by its Reynolds number, $Re = \frac{\rho U D}{\mu}$, where the characteristic length is the cylinder diameter, $D$. For $Re \leq 188.5$ the flow is 2D and wholly laminar, but for $Re \geq 47$ the flow is unsteady.

With 31,640 elements and a time-step of $dt = \frac{1}{30}T = \frac{1}{30}\frac{D}{USt}$, where $T$ is the vortex shedding period and $St$ is the Strouhal number, the model is sufficiently mesh and time independent for $Re \leq 180$ (see (9)). Here, the control was ramped up over $1T$ on a fully-developed solution of the uncontrolled flow. The simulation was run until the flow was fully-developed again (usually $10T$). The unsteady studies always commenced using a fully-developed uncontrolled flow as the initial condition.

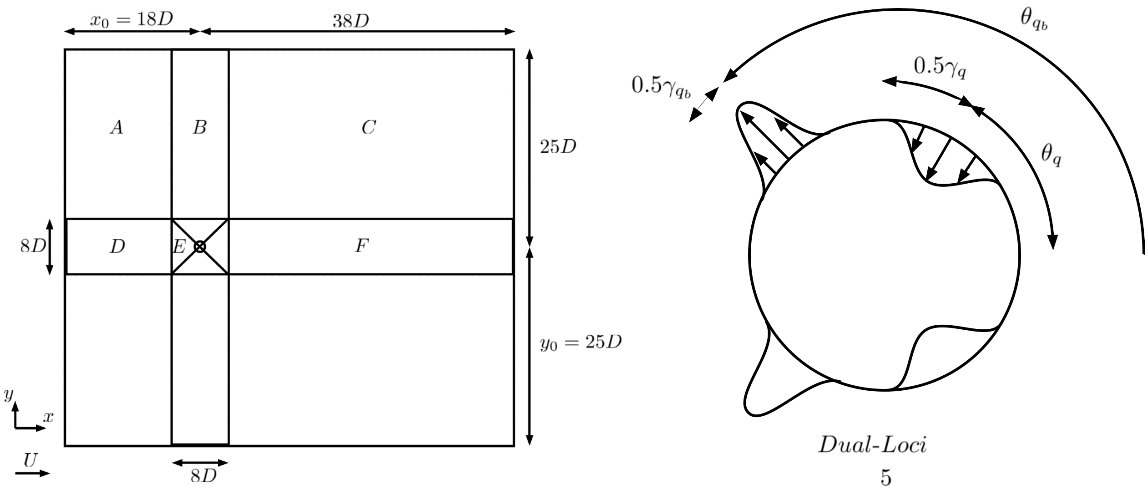


Figure 1: Computational domain for simulations (a); Schematic illustrating the key parameters for the dual-loci control. The subscript '$b$' denotes a blowing control parameter, while no subscript indicates suction (b).

### Boundary Conditions

The numerical boundary conditions consist of a uniform inlet on the left, lower and upper boundaries, $u = U = \frac{Re\nu}{D}$, $v = 0$. A zero relative pressure outlet is defined on the right boundary. The boundary on the cylinder was defined with a prescribed velocity Dirichlet condition. Suction and blowing profiles were implemented through this boundary condition as a function of angle from the trailing edge, $\theta$. Theoretically infinite suction/blowing profiles could be implemented, however it was found in (9) that optimal suction in this range typically consisted of a single locus of suction. A bell-shaped (cubic) profile was effective. Hence, in this work varieties of this 'single locus' profile for the suction and blowing profiles were considered, and with suction/blowing in the normal direction only ($\mathbf{u} = (u_n, u_t) = (u_n, 0)$ at the cylinder wall).

The suction/blowing profiles on the cylinder were defined to have one area (locus) of suction and one locus of blowing. This is called the 'dual-loci' approach in this paper. Each control locus utilises the 'single locus' profile from (9) which defines a smooth cubic profile with zero derivatives at its centre and edge. Three parameters are needed to define the profile: the location of the locus centre as measured from the trailing edge (TE), $\theta_q$, the spread of the locus measured as an angle, $\gamma_q$, and the maximum strength (which is applied at the centre, $c_{q_{max}}$. These are illustrated in Figure 1. By superimposing two single locus profiles – one for blowing, one for suction – the dual-loci control is achieved. The control applied is mirrored across the streamwise axis of the cylinder.

**Outline of Studies**
The results of two studies on autogenous suction control are presented here:

1. Q-balanced control: flow-rates of the suction and blowing loci must be equal ($Q_s = Q_b$), but no pressure requirement is imposed.

2. P-Q-balanced control: Flow-rates must be equal and the pressure gradient negative from suction to blowing ($Q_s = Q_b$, $P_s - P_b \geq 0$).

The first represents a case where a pump or other device must be used in order to produce the suction/blowing, whereas the second is the autogenous case.

**Optimisation Approach**
**Control Parameters**
In each model there were five independent control parameters and one dependent control parameter as summarised in Table 1. As $Q_s$ must equal $Q_b$ to maintain continuity, the sixth control parameter ($c_{q_{max_b}}$) is dependent on the rest.

Table 1: Control Parameters

| Parameter Name | Suction Parameter | Blowing Parameter |
|---|---|---|
| Control angle (°) | $0 \leq \theta_q \leq 180$ | $0 \leq \theta_{q_b} \leq 180$ |
| Control spread (°) | $0 \leq \gamma_q \leq 90$ | $0 \leq \gamma_{q_b} \leq 90$ |
| Control peak strength | $0 \leq c_{q_{max}} \leq 1$ | $c_{q_{max_b}} = \frac{\gamma_{q_s}}{\gamma_{q_b}} c_{q_{max}}$ |

**Objectives and Constraints**
The major control objective in each study was to minimise the total drag on the cylinder as evaluated by integrating the stream-wise normal and shear forces:

$$J_{d_t} = C_{d_t} = C_{d_p} + C_{d_f} = \frac{1}{\frac{1}{2}\rho U^2 D} \oint \left( -p(\theta) + \mu \frac{-\partial u_t(\theta)}{\partial r} \right) \cos(\theta) R d\theta, \tag{3}$$

where $R$ the radius of the cylinder, and $\theta$ the angle measured anti-clockwise from the trailing edge.
For the autogenous control studies (Model III), an additional objective that the averaged suction pressure must be greater than the averaged blowing pressure was included:

$$J_{auto} = \Delta P = P_s - P_b \geq 0. \tag{4}$$

The suction and blowing parameters were optimised with a nested approach, as shown in Figure 2. I.e. the suction control parameters are selected by the control algorithm, then a secondary optimisation occurs to arrange the blowing locus such that the drag is minimised and pressure drop maximised for that particular suction arrangement. The major optimisation then evaluates how well this combined suction/blowing control achieves the total objectives. The inner (minor) optimisations had a maximum of 50 model evaluations each time it was called.

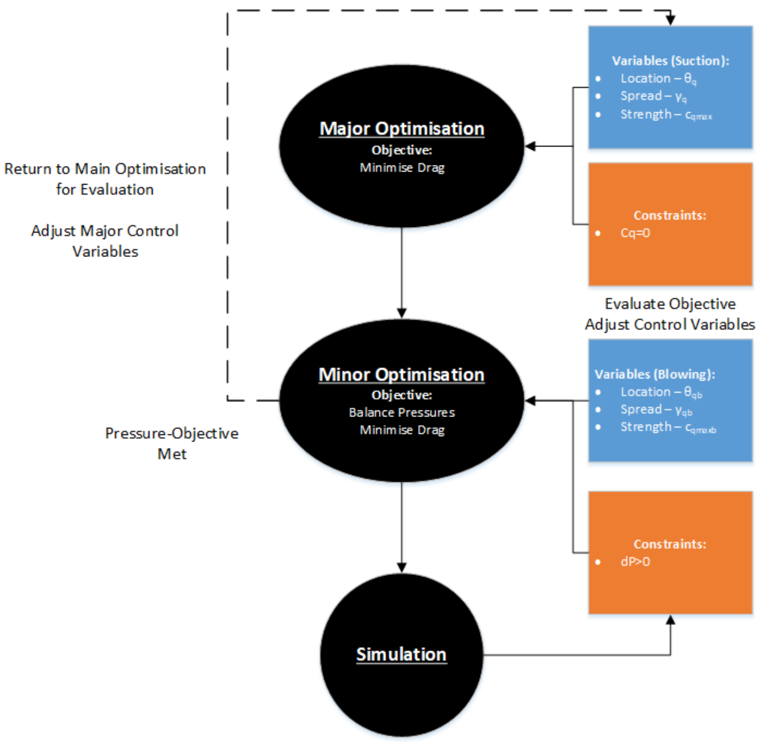


Figure 2: Flow-chart of P-Q-Balanced Dual-Loci optimisation (autogenous suction control).

An additional constraint was also implemented, preventing the suction and blowing loci from overlapping in order to generate realisable controls.

## Results & Discussion

### Optimisation of Non-Autogenous Dual-Loci Control

Optimisation of the Q-balanced dual-loci control resulted in suction/blowing control which reduced drag by up to 13% at $Re = 40$ and 22% at $Re = 120$. The control parameters and key results for the optimised control summarised in Table 2 and Table 3 while the velocity and pressure contours are shown in Figure 3. The improvement in drag is strong at both $Re$, but more potent at the higher Reynolds number of $Re = 120$. However, when the pressure differential between the suction and blowing loci are considered ($-dP = -1.5387\& - 1.4143$), it can be seen that this control would require substantial power to run due to the strong APG between the suction and blowing loci.

The optimised control profiles feature suction upstream and blowing near the trailing edge of the cylinder. The suction removes the low momentum fluid and entrains higher momentum which delays the separation. Consequently the pressure drag is greatly reduced, while there is a smaller increase in skin friction drag due to the now higher velocity gradient at the wall. At both Reynolds numbers there is a narrow spread for the suction and a wider spread for blowing. This reflects the previous findings shown in (9) where the drag is very sensitive to the location of suction - with clearly advantageous locations. Therefore, the most efficient control targets these locations. Similarly, it appears that the trailing edge is the best location for blowing control. This helps to increase the base pressure.

Table 2: Key control parameters for drag-optimised Q-balanced dual-loci control compared to its unbalanced variety.

| Parameter | $Re = 40$ | Re=120 |
|---|---|---|
| $\theta_q$ | 97.898° | 78.897° |
| $\gamma_q$ | 31.676° | 43.607° |
| $c_{q_{max}}$ | 0.987 | 0.569 |
| $\theta_{q_b}$ | 31.501° | 27.835° |
| $\gamma_{q_b}$ | 63.001° | 55.669° |
| $c_{q_{max_b}}$ | -0.496 | -0.446 |
| $C_q$ | 0 | 0 |

Table 3: Key results for optimised Q-balanced control compared to uncontrolled case.

| Parameter | $Re = 40$ | | $Re = 120$ | |
|---|---|---|---|---|
| | No Control | Q-Balanced | No Control | Q-Balanced |
| $C_{d_t}$ | 1.6321 | 1.4158 | 1.0860 | 0.8486 |
| $C_{d_p}$ | 1.0760 | 0.4365 | 0.8177 | 0.1998 |
| $C_{d_f}$ | 0.5561 | 0.9793 | 0.2683 | 0.6487 |
| $\theta_s$ | 54.107° | 37.809° | 68.826° | 32.612° |
| $dP$ | - | -1.5387 | - | -1.4143 |

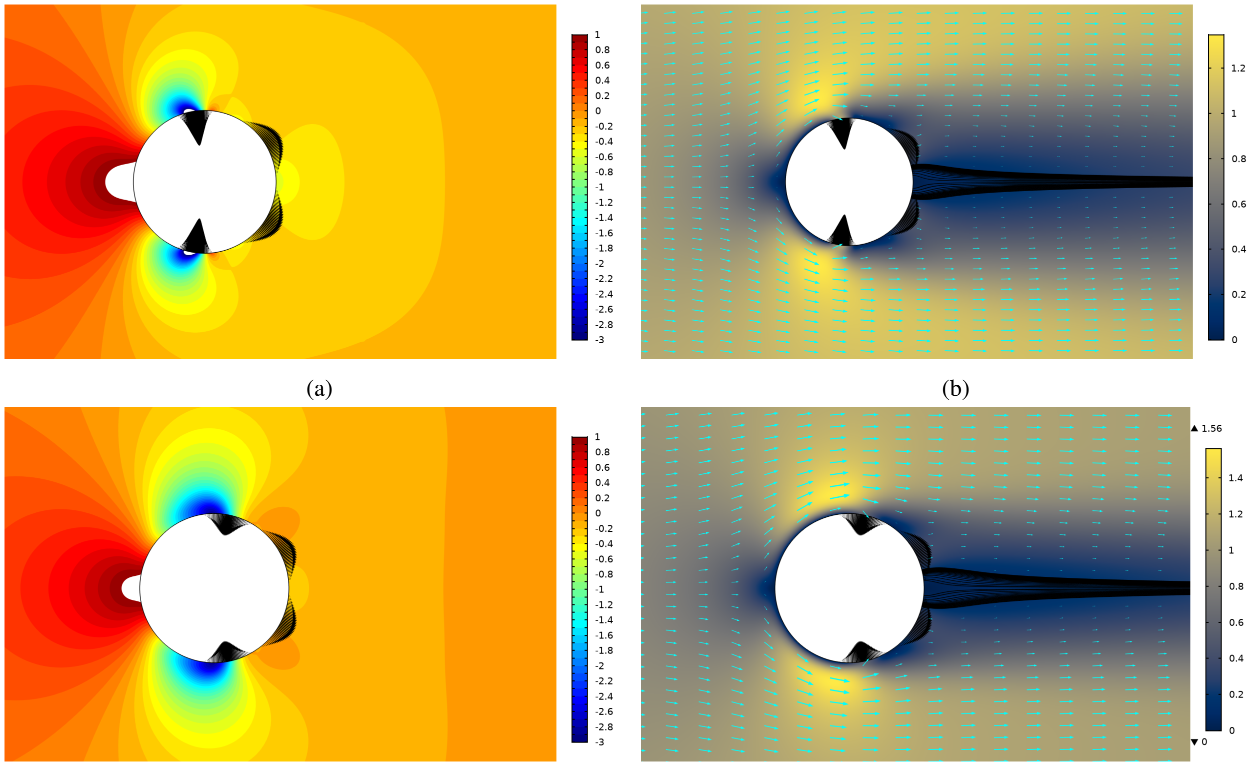

(a) (b) (c) (d)

Figure 3: Velocity surface (a,c) and pressure contours (b,d) for optimised Q-balanced dual-loci controlled flow at $Re = 40$ (a,b) and $Re = 120$ (c,d).

## Time-Dependent Simulation Verification

Time-Dependent Simulation Verification

The key results for best non-autogenous control from the optimisation study at $Re = 120$ are shown in Table 4. This optimised control is strong enough to fully stabilise the flow, therefore the results from the steady-state simulations match perfectly with the time-dependent simulations. However, since this control should be compared against the drag for the time-dependent case, the improvement is now seen to be 38.7%. The data in Table 6 clearly indicates that this massive improvement comes from the large reduction in pressure drag, while the skin friction drag has almost doubled. The control arrangement is still highly unfavourable for autogenous control, and its actual efficiency would be low given the large adverse pressure gradient (APG) that the control flow has to overcome. However, it is encouraging to see that the dual-loci control can be extremely effective on unsteady flows. The pressure and velocity contours are not shown for this simulation as they match in practically every aspect, those in Figure 3.

Table 4: Key results for optimised Q-balanced dual-loci control verified on time-dependent simulations at $Re = 120$.

| Parameter | No Control (SS) | No Control (TD) | Q-Opti (SS) | Change from No Control SS (%) | Q-Opti TD | Change from No Control TD (%) |
|---|---|---|---|---|---|---|
| $C_{d_t}$ | 1.086 | 1.3851 | 0.8486 | -21.90% | 0.8486 | -38.70% |
| $C_{d_p}$ | 0.8177 | 1.0585 | 0.1998 | -75.60% | 0.1997 | -81.10% |
| $C_{d_f}$ | 0.2683 | 0.3266 | 0.6487 | 141.80% | 0.6489 | 98.70% |
| $dP$ | - | - | -1.414 | - | -1.415 | - |

**Optimisation of Autogenous Dual-Loci Control**
**Steady-State Optimisation**

Using the two-optimisation process, the dual-loci control was successfully optimised to minimise drag while enforcing the constraint on pressure drop between the suction and blowing loci.The optimised control parameters and key results are shown in Tables 6 to 8.

The improvement in drag is much weaker when the autogenous constraint is imposed compared to the Q-balanced approach above. Nevertheless, the drag on the cylinder was reduced while maintaining a positive pressure gradient from the suction to blowing loci. In other words, autogenous suction control was effective for this flow. It was found that the optimised control was quite sensitive to the initial control parameter values for this flow, so two sets of initial values were used at both $Re$ - IV1 and IV2 as described in Table 5. For IV1, at $Re = 40$ the drag was reduced by $5.45\%$ while at $Re = 120$ a more modest $3.68\%$ improvement was achieved while the improvements from the IV2 case were even lower.

Table 5: Initial values of control parameters for P-Q-balanced dual-loci optimisation.

| **Control parameter** | **Initial Values (IV1)** | **Alternative Initial Values (IV2)** |
|---|---|---|
| $\theta_q$ | 150° | 120° |
| $\gamma_q$ | 20° | 40° |
| $c_{q_{max}}$ | 0.1 | 0.1 |
| $\theta_{q_b}$ | 90° | 80° |
| $\gamma_{q_b}$ | 10° | 10° |
| $c_{q_{max_b}}$ | -0.2 | -0.4 |

In both cases, the drag improvement was through a combination of the pressure drag and skin friction drag. This is unlike for the case of suction only or Q-balanced control, where the pressure drag is substantially improved but the skin friction worsened to produce a net benefit. At both Reynolds numbers, a quite different control flow was utilised to achieve the drag objective. This was to produce a suction and blowing very close to each other on the front half. This is effective at manipulating the $C_f$ and $C_p$ profiles over the front half, reducing the pressure and skin friction, rather than delaying separation or improving the base pressure.

This dramatically different control arrangement appears to be a factor of the initial values provided for the control. When alternative initial values – IV2 – were used, the resulting control was quite different. The final optimised controls were very similar to their initial conditions which suggests that there are other local optima that may be found also.

Table 6: Optimised control values for different dual-loci settings.

| | $Re = 40$ | | $Re = 120$ | |
|---|---|---|---|---|
| Parameters | P-Q-Balanced | Q-Balanced | P-Q-Balanced | Q-Balanced |
| $\theta_q$ | 165.520° | 97.898° | 165.260° | 78.897° |
| $\gamma_q$ | 26.015° | 31.676° | 27.158° | 43.607° |
| $c_{q_{max}}$ | 0.381 | 0.987 | 0.162 | 0.569 |
| $\theta_{q_b}$ | 144° | 31.501° | 146° | 27.835° |
| $\gamma_{q_b}$ | 10° | 63.001° | 4.410° | 55.669° |
| $c_{q_{max_b}}$ | -0.99 | -0.496 | -1 | -0.446 |
| $C_q$ | 0 | 0 | 0 | 0 |

Table 7: Optimised control values for different dual-loci settings.

| Parameter | $Re = 40$ | | | $Re = 120$ | | |
|---|---|---|---|---|---|---|
| | No Control | Q-Balanced | P-Q-Balanced | No Control | Q-Balanced | P-Q-Balanced |
| $C_{d_t}$ | 1.6321 | 1.4158 | 1.5432 | 1.086 | 0.8196 | 1.046 |
| $C_{d_p}$ | 1.076 | 0.4365 | 1.03 | 0.8177 | 0.1265 | 0.8013 |
| $C_{d_f}$ | 0.5561 | 0.9793 | 0.51316 | 0.2683 | 0.6931 | 0.2447 |
| $\theta_s$ | 54.107° | 37.809° | 176.08 | 68.826° | 29.392° | 147.74 |
| $dP$ | -1.6333 | -1.5387 | 0.3403 | - | -1.4143 | 0.4928 |

Table 8: Change in optimised result depending on initial values for control at $Re = 40$ and $Re = 120$.

| Parameters | IV1 | Re=40 Opti | Re=120 Opti | IV2 | $Re = 40$ Opti | $Re = 120$ Opti |
|---|---|---|---|---|---|---|
| $\theta_q$ | 150° | 165.52° | 165.26° | 120° | 119.96° | 121.91° |
| $\gamma_q$ | 20° | 26.015° | 27.158° | 40° | 42.566° | 51.7° |
| $c_{q_{max}}$ | 0.1 | 0.3807 | 0.16239 | 0.1 | 0.111 | 0.053 |
| $\theta_{q_b}$ | 90° | 144° | 146° | 80° | 24.313° | 39.5° |
| $\gamma_{q_b}$ | 10° | 10° | 4.4102° | 10° | 47.125° | 23.5° |
| $c_{q_{max_b}}$ | -0.2 | -0.9904 | -1 | -0.4 | -0.1002 | -0.1176 |
| $dP$ | - | 0.3403 | 1.046 | - | 0.0277 | 1.077 |
| $C_{d_t}$ | - | 1.5432 | 0.8013 | - | 1.6083 | 0.7716 |

The pressure contour and velocity surfaces are shown for the best optimised P-Q-Balanced dual-loci control (IV1 case) below at $Re = 40$ & 120 in Figure 4. The control is concentrated on the front-half and improves both the skin friction and pressure drag modestly. This control arrangement is highly dependent on the initial values used for the optimisation study.

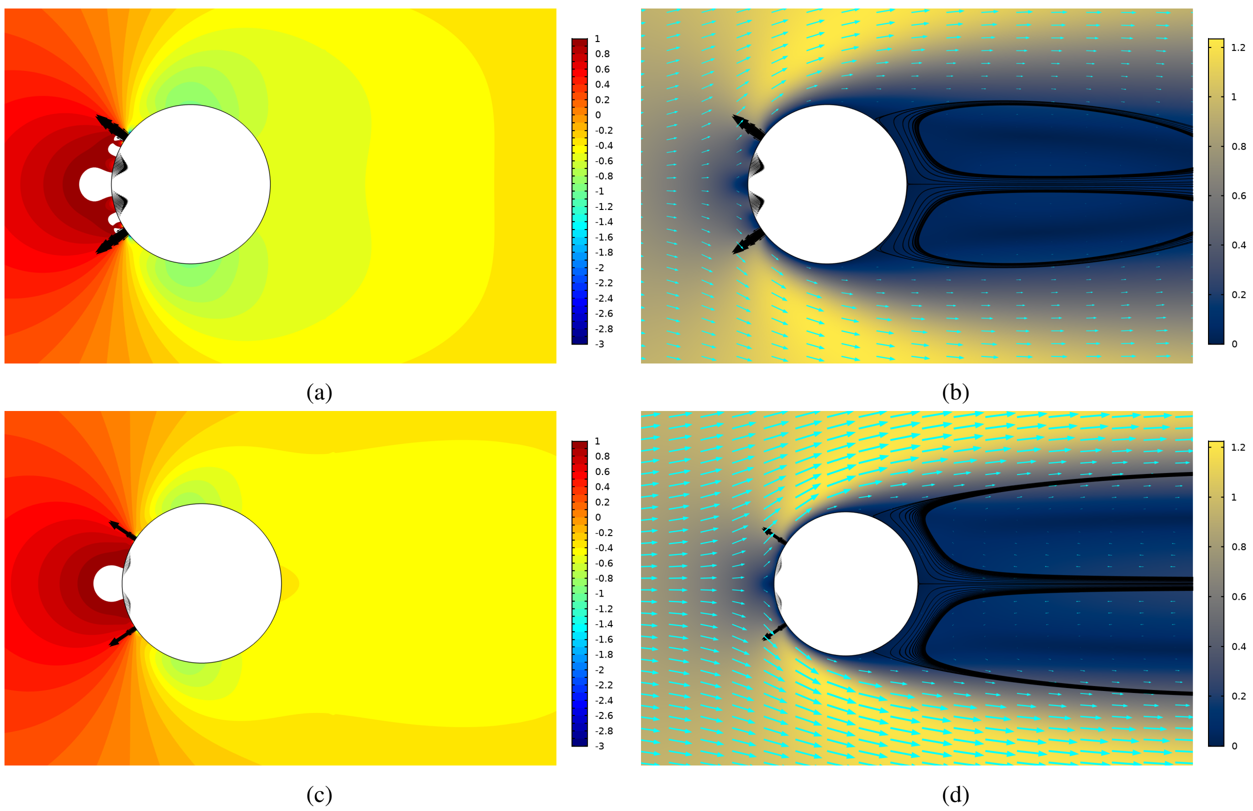


Figure 4: Velocity surface (a,c) and pressure contours (b,d) for optimised P-Q-balanced dual-loci controlled flow round cylinder at $Re = 40$ (a,b) and $Re = 120$ (c,d).

Overall, the major research question of "can autogenous suction control theoretically be used to reduce drag for bluff body flows?" has been found to be true. Certainly for $Re = 40$, whereas the flow at $Re = 120$ should be resolved with an unsteady simulation to confirm.

**Time-Dependent Verification**

As for the non-autogenous Q-balanced control, to verify whether these results are feasible for the true unsteady flow at $Re = 120$, time-dependent simulations were carried out with the optimised control parameter. These simulations were successful and found that the optimised controls still satisfied the pressure-drop requirements in both time-dependent cases. Unlike for the Q-balanced control, the optimised autogenous control does not stabilise the flow at $Re = 120$ and therefore the steady-state simulations are flawed. The time-averaged values (over one vortex-shedding period), and their fluctuation are given for the key parameters of the first P-Q-balanced design compared to the steady-state values in Table 9. The key parameters for both P-Q-balanced designs are provided in Table 10.

As expected, the drag coefficient values are quite different from the steady-state values, but the reaction to the control is consistent in the TD simulations. For the first optimised arrangement (with the suction and blowing situated at the front of the cylinder), the improvement in drag is dulled. An average $2.5\%$ improvement was produced compared to the $3.7\%$ predicted by the steady-state study. Importantly, the positive pressure gradient between the suction and blowing loci remains, and in fact is greater for the TD case ($0.5764$ vs. $0.4928$). This makes sense as the pressure profile is steeper and has a larger fluctuation for the unsteady case, even for the uncontrolled flow, which is beneficial for the autogenous constraint.

The most interesting result is the dramatic change in performance for the second P-Q-balanced design (produced using the second set of initial values in the optimisation). Where the steady-state result suggested a reduction in drag of only $0.83\%$, the actual result when applied to the unsteady cylinder flow was actually $4.3\%$. This is not just better than the SS estimate, but it is a greater improvement than the first P-Q-balanced design. While the first design reduces both skin friction and pressure drag modestly, the second design uses the same mechanisms as suction-only control to minimise total drag by greatly reducing the pressure drag at the cost of slightly increasing the skin friction drag. The design of this control fits better with previous findings that suction near the $90°$ mark with blowing situated near the rear produces the best drag-reduction but is difficult to achieve with autogenous pressure gradients (5).

Table 9: Key results for SS-optimised P-Q-balanced dual-loci control applied to time-dependent simulation compared to the steady result and uncontrolled values. SS= steady-state, TD= time-dependent.

| Parameter | SS No Control | SS P-Q Opti | TD No Control Average | TD P-Q Average | TD P-Q Fluctuation (±) | % Change |
|---|---|---|---|---|---|---|
| $C_{d_t}$ | 1.086 | 1.046 | 1.3851 | 1.3517 | 0.0169 | $-2.50\%$ |
| $C_{d_p}$ | 0.8177 | 0.8013 | 1.0585 | 1.0485 | 0.0155 | $-1.00\%$ |
| $C_{d_f}$ | 0.2683 | 0.2447 | 0.3266 | 0.3032 | 0.0017 | $-7.70\%$ |
| $dP$ | - | 0.4928 | - | 0.5764 | 0 | - |

Table 10: Comparison of the two optimised P-Q-Balanced dual-loci control in full time-dependent simulation.

| Parameter | TD No Control Average | TD Fluctuation (±) | IV1 TD P-Q Average | IV1 TD P-Q Fluctuation (±) | IV2 TD P-Q Average | IV2 TD P-Q Fluctuation (±) |
|---|---|---|---|---|---|---|
| $C_{d_t}$ | 1.3851 | 0.0171 | 1.3517 | 0.0169 | 1.3274 | 0.0096 |
| $C_{d_p}$ | 1.0585 | 0.0156 | 1.0485 | 0.0155 | 0.9715 | 0.0088 |
| $C_{d_f}$ | 0.3266 | 0.0017 | 0.3032 | 0.0017 | 0.356 | 0.0008 |
| $dP$ | - | - | 0.5764 | 0 | 0.0747 | 0.0027 |

This second arrangement of the autogenous suction control is particularly promising for a variety of reasons. Firstly, the control flow rates are much lower. While the relationship between the control flow rate and the necessary pressure to drive it has mostly been ignored in the present study, it is likely that large control flows will require larger pressure drops. The peak suction strength is only $c_{q_{max}} = 0.053$ which is more like the level of suction seen for early boundary layer studies (23, p. 383). Secondly, the flow-path for the control is better. While the optimisation procedure accounts for the effects of blowing control on the boundary layer and the second-order impact on the pressure profile, it seems logical to have the flow exhausted out the rear of the cylinder. This prevents the boundary layer from being blown away, and does not have to produce a dramatic change in the momentum direction of the control flow. Finally, the second control arrangement appears to dampen the dynamics of the flow. The fluctuations of the drag coefficients are all reduced from the uncontrolled case. The time-averaged flow fields are shown for the two controlled and uncontrolled cases in Figure 5.

The changes to the flow are subtle so there is little to remark on except the small morphing of the reversed flow region in the wake from the blowing in the second case.

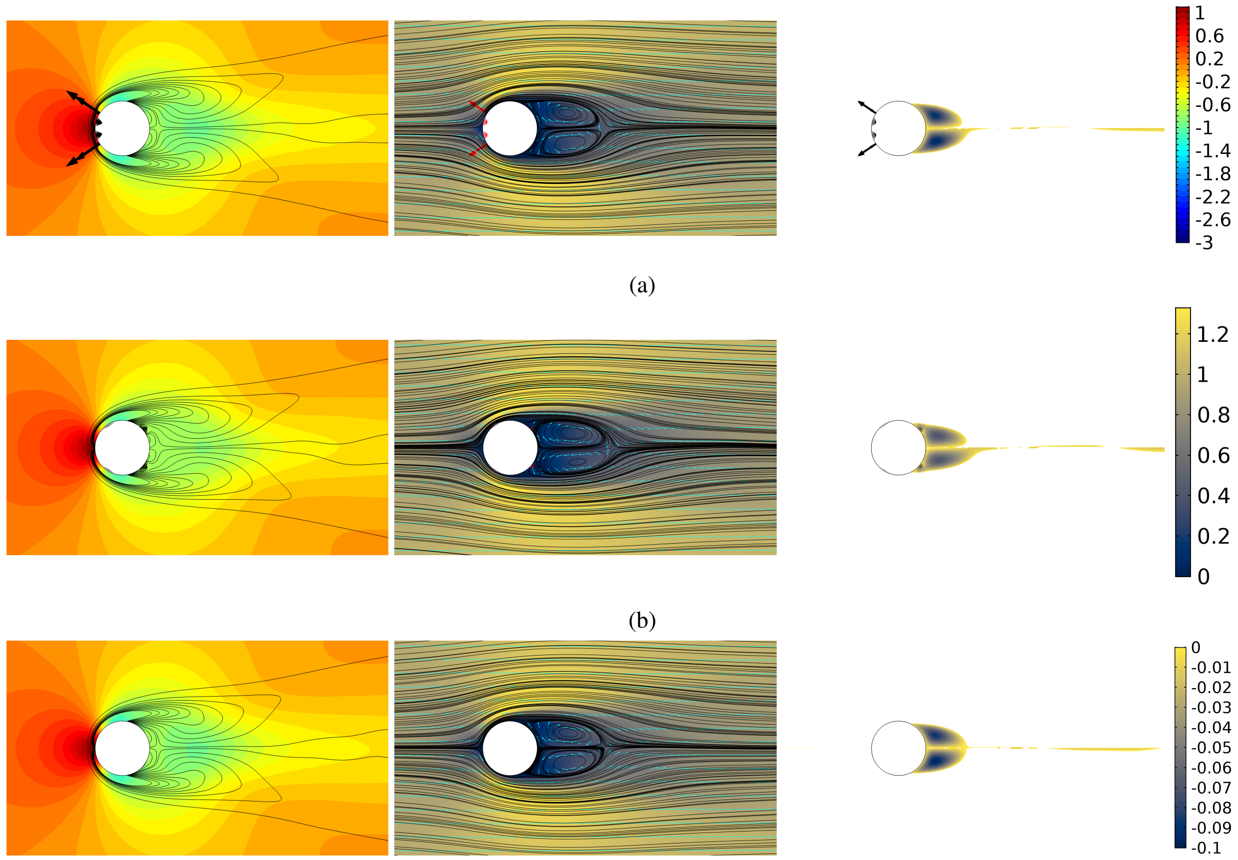


(a)

(b)

(c)

Figure 5: Pressure contours with vorticity streamlines (left), velocity surface with streamlines (middle) and reversed flow surfaces for the time-averaged flow round the cylinder for the IV1 optimised control (a), IV2 optimised control (b) and no control (c). Flow field is averaged over 1 vortex shedding period of the uncontrolled flow. The colour bars for the pressure, velocity and reversed flow surfaces are shown in the final column (in descending order).

## Conclusions

Numerical studies were carried out on laminar flow around a circular cylinder to develop autogenous suction control. Dual-loci control - consisting of a locus of suction and one of blowing - was imposed using velocity outlet condition on the cylinder. The parameters of this control were optimised to minimise total drag at $Re = 40$ and $Re = 120$. To impose autogenous control, a constraint that the average pressure of the suction locus is greater than or equal to that of the blowing locus. Steady-state and unsteady simulations were performed.

The optimised autogenous control was able to successfully reduce drag while maintaining the pressure gradient needed to be self-generating at both Reynolds numbers. The optimal control arrangements featured suction on the front half and blowing on the leeward half. This arrangement results in the pressure being reduced on the front half and a modest increase on the rear, resulting in a reduced pressure drag. This comes at the cost of slightly higher skin friction drag, however. Total drag was reduced by up to 4.3% at $Re = 120$ using dual-loci control with a positive pressure gradient from the suction to blowing locations, and 5.45% for $Re = 40$.

Overall the results are encouraging for the development and use of autogenous suction control in real flows. The numerical results showed improvement over the uncontrolled case, and this increased with Reynolds number. On the other hand, more work is needed. The pressure constraint is idealised - not accounting for any losses in internal ducting. The investigation successfully extended the findings of Atik and van Dommelen to show that autogenous suction control is viable for bluff body flows also.

## References

[1] Prandtl, L. (1905). Über Flüssigkeitsbewegung bei sehr kleiner Reibung. Verhandlungen des III. Internationalen Mathematiker-Kongresses, Heidelberg. LPGA, 2, 575-584.

[2] Huang, L. R., Cox, E. C., Austin, R. H., & Sturm, J. C. (2004). Continuous particle separation through deterministic lateral displacement. *Science* **304(5673)**: 987-990.

[3] Fransson, J. H., Konieczny, P., & Alfredsson, P. H. (2004). Flow around a porous cylinder subject to continuous suction or blowing. *Journal of Fluids and Structures* **19(8)**:1031-1048.

[4] Gao, D., Chen, G., Chen, W., Huang, Y., & Li, H. (2019). Active control of circular cylinder flow with windward suction and leeward blowing. *Experiments in Fluids* **60(2)**: 1-17.

[5] Min, C., & Choi, H. (1999). Suboptimal feedback control of vortex shedding at low Reynolds numbers. *Journal of Fluid Mechanics* **401**:123-156.

[6] Li, Z., Navon, I. M., Hussaini, M. Y., & Le Dimet, F. X. (2003). Optimal control of cylinder wakes via suction and blowing. *Computers & Fluids* **32(2)**:149-171.

[7] Sohankar, A., & Najafi, M. (2018). Control of vortex shedding, forces and heat transfer from a square cylinder at incidence by suction and blowing. *I*nternational Journal of Thermal Sciences **129**:266-279.

[8] Ramsay, J., Sellier, M., & Ho, W. H. (2020). Eliminating Boundary Layer Separation on a Cylinder with Nonuniform Suction. *International Journal of Aerospace Engineering* **2020**.

[9] Ramsay, J., Sellier, M., & Ho, W. H. (2020). Non-uniform suction control of flow around a circular cylinder. *International Journal of Heat and Fluid Flow* **82**: 108559.

[10] Lorite-Díez, M., Jiménez-González, J. I., Pastur, L., Cadot, O., & Martínez-Bazán, C. (2020). Drag reduction on a three-dimensional blunt body with different rear cavities under cross-wind conditions. *Journal of Wind Engineering and Industrial Aerodynamics* **200**:104145.

[11] Braslow, A. L. (1999). A history of suction-type laminar-flow control with emphasis on flight research (No. 13). NASA History Division, Office of Policy and Plans, NASA Headquarters.

[12] Choi, H., Jeon, W. P., & Kim, J. (2008). Control of flow over a bluff body. *Annu. Rev. Fluid Mech.* **40**:113-139.

[13] Atik, H., van Dommelen, L. (2008). Autogenous suction to prevent laminar boundary-layer separation. *Journal of fluids engineering* **130(1)**: 011201–1.

[14] Bahi, L., Ross, J., & Nagamatsu, H. (1983). Passive shock wave/boundary layer control for transonic airfoil drag reduction. In 21st Aerospace Sciences Meeting (p. 137).

[15] Nagamatsu, H., & FICARRA, R. (1985, January). Supercritical airfoil drag reduction by passive shock wave/boundary layer control in the Mach number range. 75 to. 90. In 23rd Aerospace Sciences Meeting (p. 207).

[16] Nagamatsu, H., Trilling, T., & Bossard, J. (1987). Passive drag reduction on a complete NACA 0012 airfoil at transonic Mach numbers. In 19th AIAA, Fluid Dynamics, Plasma Dynamics, and Lasers Conference (p. 1263).

[17] Parikh, Pradip G. "Passive removal of suction air for laminar flow control, and associated systems and methods." U.S. Patent 7,866,609, issued January 11, 2011.

[18] Wieselsberger, C. (1922). New data on the laws of fluid resistance (No. NACA-TN-84).

[19] Tritton, D. J. (1959). Experiments on the flow past a circular cylinder at low Reynolds numbers. *Journal of Fluid Mechanics* **6(4)**:547-567.

[20] Henderson, R. D. (1995). Details of the drag curve near the onset of vortex shedding. *Physics of Fluids* **7(9)**:2102-2104.

[21] Wu, M. H., Wen, C. Y., Yen, R. H., Weng, M. C., & Wang, A. B. (2004). Experimental and numerical study of the separation angle for flow around a circular cylinder at low Reynolds number. *Journal of Fluid Mechanics* **515**:233-260.

[22] Zdravkovich, M. M. (1997). Flow around circular cylinders: Volume 2: Applications (Vol. 2). Oxford university press.

[23] Schlichting, H. (1987). Boundary layer theory. New York: McGraw-Hill.